Journal of Power Sources 247 (2014) 219–227

Contents lists available at ScienceDirect

Journal of Power Sources

journal homepage: www.elsevier.com/locate/jpowsour

Optimal microwave-assisted hydrothermal synthesis of nanosized $xLi_2MnO_3\cdot(1-x)LiNi_{1/3}Co_{1/3}Mn_{1/3}O_2$ cathode materials for lithium ion battery

Xiaowei Miao [a, b], Yuan Yan [b], Chunguang Wang [b], Leilei Cui [a], Jianhui Fang [a, *], Gang Yang [b, *]

[a] Department of Chemistry, Shanghai University, Shanghai 200444, China
[b] Jiangsu Lab of Advanced Functional Material, Changshu Institute of Technology, Changshu 215500, China

HIGHLIGHTS

- $xLi_2MnO_3\cdot(1-x)LiNi_{1/3}Co_{1/3}Mn_{1/3}O_2$ rapidly synthesized by microwave-hydrothermal method.
- The sample appears spherical morphology composed of primary spherical nanoparticles.
- Discharge capacity reaches to 325 mA h g^{-1} at 0.1 C and present good cycle performance.
- MH temperature and time play important roles in electrochemical properties of sample.

ARTICLE INFO

Article history:
Received 24 June 2013
Received in revised form
18 August 2013
Accepted 22 August 2013
Available online 3 September 2013

Keywords:
Lithium ion batteries
Cathode materials
Li-rich
Microwave hydrothermal
Cyclic performance

ABSTRACT

Li-rich layer-structure $xLi_2MnO_3\cdot(1-x)LiNi_{1/3}Co_{1/3}Mn_{1/3}O_2$ ($x = 0.2, 0.4, 0.6, 0.8$) cathode materials have been synthesized by co-precipitation and microwave hydrothermal (MH) method in a short time (~60 min). The crystal structure is characterized by X-ray diffraction (XRD) patterns, and refined by two sets of diffraction data (*R*-3*m* and *C*2/*m*). The morphology is characterized by scanning and high-resolution transmission electron microscope (SEM and HRTEM) which shows the average particle size (50–100 nm). The charge/discharge results indicate $xLi_2MnO_3\cdot(1-x)LiNi_{1/3}Co_{1/3}Mn_{1/3}O_2$ ($x = 0.4$) synthesized at 180 °C for 60 min has the best discharge capacity and cyclic performance. Within the cut-off voltage between 2.5 and 4.8 V, the initial discharge capacity is 325 mA h g^{-1} at 0.1 C rate; and after 50 cycles the discharge capacity remains 234.5 mA h g^{-1}. The $xLi_2MnO_3\cdot(1-x)LiNi_{1/3}Co_{1/3}Mn_{1/3}O_2$ prepared by facile and rapid microwave-assisted hydrothermal (MH) is a promising preparation method in cathode material for lithium ion batteries.

1. Introduction

With the increasing global energy demand, the rechargeable lithium-ion batteries have been intensively investigated as a power source for electric vehicles (EVs) and hybrid electric vehicles (HEVs) over the past few years [1–3]. One of specific requirements is positive electrode material with high capacity, low cost and environmental. Lithium cobalt oxide was the first to be utilized as a positive electrode for commercial lithium secondary batteries, but its high cost, toxicity and poor high-rate capacity limit its use in large-scale applications, such as EVs and HEVs.

Recently, Li-rich cathodes written as $Li_{1+x}[M]_{1-x}O_2$ (M: Mn, Ni, and Co; $x > 0$) have caught the great attention for the novel electrode materials of lithium ion batteries [4]. These materials with low content of cobalt and high Mn content are low cost and lead to interesting capacities, up to 250 mA h g^{-1} or more [5]. The currently used cathodes for lithium-ion batteries, $LiCoO_2$, $LiFePO_4$ and $LiNi_{1/3}Co_{1/3}Mn_{1/3}O_2$ deliver the capacities of 140, 170, and 160 mA h g^{-1}, respectively [6–8]. However, Li-rich cathodes weren't completely understood in terms of the structural features and electrochemical behaviors. The Li-rich cathode material $Li_{1+x}[M]_{1-x}O_2$ (M: Mn, Ni, and Co; $0 < x < 1$) can be considered as a solid-solution between $LiMO_2$ (M = Ni, Co, Mn, etc.) based on the α-$NaFeO_2$ type structure (*R*-3*m* space group) and Li_2MnO_3 (*C*2/*m* space group) structure. Many studies have been performed to explain these integrated layered systems [9–12]. $LiMO_2$ (M = Ni, Co, Mn, etc.) can be described as layers of MO_6 octahedra (so called "slabs") and

* Corresponding authors.
E-mail addresses: jhfang@shu.edu.cn (J. Fang), gyang@cslg.edu.cn, gangyang@ua.pt (G. Yang).

0378-7753/$ – see front matter © 2013 Elsevier B.V. All rights reserved.
http://dx.doi.org/10.1016/j.jpowsour.2013.08.097

Li_2MnO_3 alternatively stacked with layers of LiO_6 octahedra ("insterslabs") [$Li_{1/3}Mn_{2/3}$] slabs [13–15]. In these compounds, Li_2MnO_3 and Li_2MnO_3-like domains exist with short-range order within a $LiMO_2$ matrix [16]. The component of Li_2MnO_3 is significantly important because it can remain the structural stability and provide additional high capacity to electrode by simultaneously extracting the lithium ions with the release of oxygen and a net loss of Li_2O at potential above 4.5 V [17–19].

The drawbacks of these series of materials are their huge irreversible capacity loss, dramatic capacity fading and poor rate capability [20]. To overcome such shortcomings of Li-rich layer cathode material, different synthesis methods were employed to control the morphology and improve the electrochemical performance, for instance, co-precipitation [21,22], sol–gel and conventional hydrothermal [23]. Kim et al. [24] synthesized $0.3Li_2MnO_3\cdot0.7LiMn_{1-x}Ni_yCo_{0.1}O_2$ ($x = 0.3$, $y = 0.2$) by co-precipitation which in the voltage region of 2.0–4.6 V delivered initially capacity of about 200 mA h g^{-1} at 0.1 C and exhibits a poor cycle life. S.-H. Kang et al. [25] synthesized $0.5Li_2MnO_3\cdot0.5LiNi_{0.44}Co_{0.25}Mn_{0.31}O_2$ by sol–gel method which showed reversible capacities of 250 mA h g^{-1} at C/11 rate, 225 mA h g^{-1} at 0.5 C and 200 mA h g^{-1} at 1 C, respectively. Among the above synthesis methods, the conventional hydrothermal process is a good way to control the chemical composition, crystal size and morphology of Li-rich cathode materials. For example, nanosized $LiMnO_2\cdot Li_2MnO_3$ compounds were synthesized via a hydrothermal method by Y. Yang et al. [26], which delivered a capacity of 208 mA h g^{-1} at a current density of 200 mA g^{-1}. But the long hydrothermal time limits the wide application to synthesize cathode material for lithium ion batteries. In this regard, temperature-controlled microwave hydrothermal (MH) method was considered, which was ever used to synthesize cathode material, such as $LiMnO_2$ [27], $LiMPO_4$ (M = Fe, Mn, Co) [28], $LiFePO_4$ [29]. By comparison with traditional hydrothermal preparation, microwave irradiation play two important roles in thermodynamic and kinetic, heating the reaction system to reach to the hydrothermal temperature and accelerating the ions diffusion ability to improve the reaction rate. Owning to the intrinsic heating characteristics increasing the kinetics of reaction, the reaction time via microwave-assisted hydrothermal is less than 10% of conventional hydrothermal method. In addition, the microwave-assisted hydrothermal process is particularly successful with respect to controlling the chemical composition, crystal size, and particle morphology. Until now, the synthesis of Li-rich cathode materials via microwave hydrothermal method has not been reported yet.

In this work, we have successfully synthesized the cathode material $xLi_2MnO_3\cdot(1-x)LiNi_{1/3}Co_{1/3}Mn_{1/3}O_2$ ($x = 0.2, 0.4, 0.6, 0.8$) by microwave hydrothermal (MH) method in a short time (~60 min). The as-synthesized $xLi_2MnO_3\cdot(1-x)LiNi_{1/3}Co_{1/3}Mn_{1/3}O_2$ ($x = 0.4$) reach to the maximum discharge capacity of 325 mA h g^{-1} at 0.1 C and present good cycle performance. The synthesis, structures and electrochemical performance in relations of different molar ratio (x) of $Li_2MnO_3/LiMO_2$, MH temperature and time were systematically optimized and discussed in detail.

2. Experimental section

2.1. Material synthesis

The $xLi_2MnO_3\cdot(1-x)LiNi_{1/3}Co_{1/3}Mn_{1/3}O_2$ ($x = 0.2, 0.4, 0.6, 0.8$) cathode material was synthesized by microwave hydrothermal method using manganese–nickel–cobalt hydroxide precursor. The precursor was prepared by a co-precipitation method from 0.5 mol dm^{-3} of $NiAc_2\cdot4H_2O$, $CoAc_2\cdot H_2O$, $MnAc_2\cdot4H_2O$ aqueous solution and 0.7 mol dm^{-3} of LiOH aqueous solution. The right amount of $NH_3\cdot H_2O$ was added to keep the PH of the mixed solution in the range of 11–12 during the precipitation process. The solution were mixed by means of burette in a nitrogen filled container with high speed stirring about 2000 rpm for 8 h. The mixture was transferred into a 70 mL polytetrafluoroethylene (PTFE) vessel. MH treatment was program-controlled in the microwave digestion system (MDS-6 Shanghai Sineo) for different reaction of temperature and time. After the vessel was cooled down, the dark chocolate-brown precipitate was collected, washed with distilled water for several times and dried. Finally, the MH products were heated at 800 °C for 3 h in air atmosphere.

A series of products were synthesized under different microwave hydrothermal conditions: (1) The MH temperature and time are fixed at 180 °C and 60 min, and the molar ratios of x are variable. The products are referred to as 0.2LMO/LNCM_180C/60m (0.2 means molar ratio of Li_2MnO_3/LMO_2, LMO is on behalf of Li_2MnO_3, LNCM is on behalf of $LiNi_{1/3}Co_{1/3}Mn_{1/3}O_2$, 180C means MH under 180 °C, 60m means MH for 60 min. The following abbreviations are identical), 0.4LMO/LNCM_180C/60m, 0.6LMO/LNCM_180C/60m and 0.8LMO/LNCM_180C/60m, respectively. (2) The molar ratio of x and MH time are fixed as $x = 0.4$ and 60 min, the MH temperatures are 160, 180 and 200 °C, respectively. The products are named as 0.4LMO/LNCM_160C/60m, 0.4LMO/LNCM_180C60m and 0.4LMO/LNCM_200C/60m. (3) The molar ratio of x and MH temperature are fixed as $x = 0.4$ and 180 °C, the MH times are 30, 45, and 60 min, respectively. The products are named as 0.4LMO/LNCM_180C/30m, 0.4LMO/LNCM_180C/45m and 0.4LMO/LNCM_180C/60m. As a comparison, $xLi_2MnO_3\cdot(1-x)LiNi_{1/3}Co_{1/3}Mn_{1/3}O_2$ ($x = 0.4$) is synthesized by traditional hydrothermal (TH) processes. The precursor mixture was transferred into a 100 mL polytetrafluoroethylene (PTFE) autoclave and reacted in the electric oven at 180 °C for 48 h. The as-synthesized sample is simply named as TH_0.4LMO/LNCM_180C/48h.

2.2. Material characterization

X-ray studies are done on a Rigaku diffractometer with Cu K_a radiation. The diffraction data are collected from 10 to 80°, with a step size of 0.02° and a count time of 4 s. The crystal structure parameters of the samples $xLi_2MnO_3\cdot(1-x)LiNi_{1/3}Co_{1/3}Mn_{1/3}O_2$ ($x = 0.2, 0.4, 0.6, 0.8$) were refined by Rietveld analysis through using the General Structure Analysis System (GSAS) [30]. The crystal morphology was characterized by scanning electron microscope (SEM, Hitachi-X650 microscope, 20 kV) and high-

Table 1
The specific surface area and ICP analysis of $xLi_2MnO_3\cdot(1-x)LiNi_{1/3}Co_{1/3}Mn_{1/3}O_2$ with different ratio of x.

Samples	BET	Content (ppm)				Theoretical molar ratio of Li:Ni:Co:Mn				Calculated molar ratio of Li:Ni:Co:Mn			
	(m^2 g^{-1})	Li	Ni	Co	Mn								
0.2LMO/LNCM_180C/60m	5.98	0.9096	1.3040	1.2780	2.0890	1.20	0.27	0.27	0.47	1.61	0.27	0.27	0.46
0.4LMO/LNCM_180C/60m	9.25	0.9244	1.0180	1.0460	2.9230	1.40	0.20	0.20	0.60	1.56	0.20	0.20	0.62
0.6LMO/LNCM_180C/60m	3.67	1.0450	0.6358	0.6291	3.2420	1.60	0.13	0.13	0.73	1.78	0.13	0.13	0.70
0.8LMO/LNCM_180C/60m	4.35	1.1160	0.3093	0.3072	3.6900	1.80	0.067	0.067	0.87	2.15	0.067	0.067	0.89

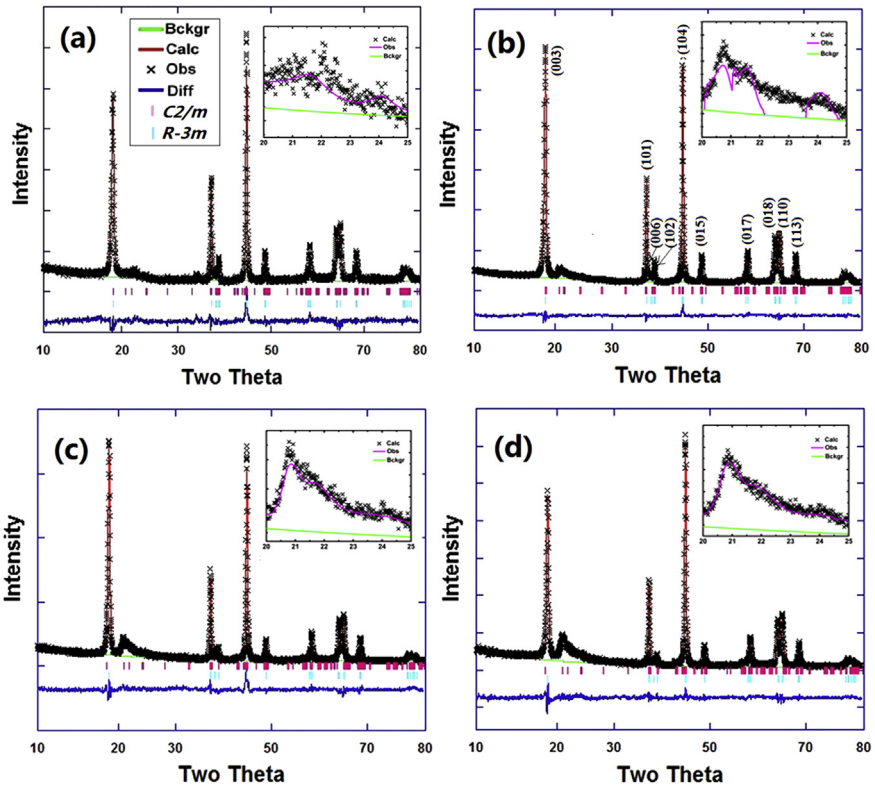

Fig. 1. Rietveld refinement results for XRD patterns of the cathode material $xLi_2MnO_3\cdot(1-x)LiNi_{1/3}Co_{1/3}Mn_{1/3}O_2$ synthesized by microwave hydrothermal at 180 °C for 60 min with different ratio of x by GSAS. (a) 0.2; (b) 0.4; (c) 0.6; and (d) 0.8.

resolution transmission electron microscope (HRTEM, JEOL-2010F, 200 kV). Elemental composition (Li, Ni, Co and Mn) of the samples was measured by ICP-OES (Inductively Coupled Plasma Optical Emission Spectrometer) (iCAP 6000). Specific surface areas were performed with a Micromeritics ASAP 2010 M + C nitrogen adsorption instrument (Micromeritics Inc., USA) at 77 K.

2.3. Electrochemical measurements

Electrochemical performances of the samples were collected in CR2016 coin cells. The positive electrodes of the active materials (80 wt%), Super P (10 wt%) and polyvinylidene fluoride (10 wt%) were mixed in *N*-methyl-2-pyrrolidone and stirred overnight. The slurry casted onto Al foil by using a doctor blade, and was dried at 120 °C for 12 h under vacuum. The electrode area was about 0.95 cm^2 and the loading density was about 2–4 mg cm^{-2}. Cells were assembled in an argon-filled glove box by using lithium metal as the negative electrode, Celgard 2500 as the separator, and 1 M $LiPF_6$ dissolved in ethylene carbonate, dimethyl carbonate and ethyl-methyl carbonate with a 1:1:1 volume ratio as the electrolyte. The galvanostatic charge and discharge tests were made at ambient temperature by using LAND CT2001A battery testing system (Wuhan, China) within the voltage range of 2.5–4.8 V vs. Li^+/Li. The cyclic voltammetry (CV) measurement was conducted on a LK2005 (Tianjin, China) electrochemical workstation at a scan rate of 0.1 mV s^{-1} in a potential range of 2.5–4.8 V (vs. Li^+/Li) at 25 °C.

3. Results and discussion

The compositions of the as-synthesized $xLi_2MnO_3\cdot(1-x)LiNi_{1/3}Co_{1/3}Mn_{1/3}O_2$ with different ratios of x were determined by ICP and listed in Table 1. The molar ratio experimentally measured for Ni, Co and Mn elements are very close to the stoichiometric values except Li. Excess Li comes into the [MnO] layer of $LiMnO_2$ transferring to the structure of Li_2MnO_3 during hydrothermal process. For example, the theoretical and calculated Li moles are 1.40

Table 2
Structure and profile parameters from the Rietveld refinement by GSAS for X-ray diffraction data of $xLi_2MnO_3\cdot(1-x)LiNi_{1/3}Co_{1/3}Mn_{1/3}O_2$ with various ratio x.

Samples		0.2LMO/LNCM		0.4LMO/LNCM		0.6LMO/LNCM		0.8LMO/LNCM	
		LMO	LNCM	LMO	LNCM	LMO	LNCM	LMO	LNCM
Lattice parameters (Å)	a	4.9576	2.8614	4.9910	2.8638	4.9486	2.8578	4.9169	2.8544
	b	8.6232	2.8614	8.5319	2.8638	8.5086	2.8578	8.5044	2.8544
	c	5.0114	14.2599	5.0260	14.2922	5.1437	14.2730	5.1650	14.2585
	c/a	1.01	4.98	1.01	4.99	1.04	4.99	1.05	4.99
Lattice volume (Å^3)		201.93	101.11	203.24	101.51	204.11	100.95	203.95	100.61
Intensity ratio	$I_{(003/104)}$	1.05		1.27		1.15		0.89	
Reliability and weighted factors	χ^2	1.85		2.35		2.07		2.06	
	Rwp/(%)	8.80		5.55		9.99		10.97	
	Rp/(%)	6.89		4.31		7.70		8.42	

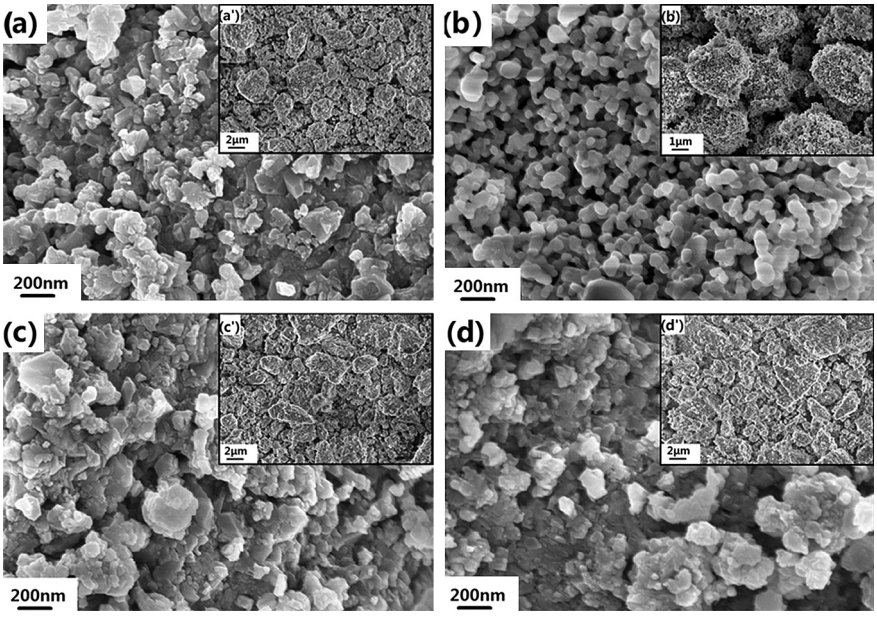

Fig. 2. SEM images of $xLi_2MnO_3\cdot(1-x)LiNi_{1/3}Co_{1/3}Mn_{1/3}O_2$ synthesized by microwave hydrothermal at 180 °C for 60 min with different ratio of x: (a) 0.2, (b) 0.4, (c) 0.6 and (d) 0.8. The insets are SEM images with lower magnification.

and 1.56 in $0.4Li_2MnO_3\cdot0.6LiNi_{1/3}Co_{1/3}Mn_{1/3}O_2$. As listed in Table 1, the Brunauer–Emmett–Teller (BET) specific surface area of $xLi_2MnO_3\cdot(1-x)LiNi_{1/3}Co_{1/3}Mn_{1/3}O_2$ at $x = 0.2$, 0.4, 0.6 and 0.8 are 5.98, 9.25, 3.67 and 4.35 $m^2\ g^{-1}$, respectively. The sample 0.4LMO/LNCM_180C/60m has the largest BET surface area.

As shown in Fig. 1, all the XRD patterns are indexed to a unit cell of α-$NaFeO_2$ type with space group *R*-3*m* and the weak peaks at $2\theta = 20–25°$ indexed to monoclinic unit cell, *C*2/*m*, that characterizes Li_2MnO_3. The magnitudes of the peaks at $2\theta = 20–25°$ increase with the increasing value x of $xLi_2MnO_3\cdot(1-x)LiNi_{1/3}Co_{1/3}Mn_{1/3}O_2$, as shown the enlarged inset image in Fig. 1. As shown in Fig. 1 and Table 2, the character peak intensities of XRD patterns and the value of c/a are dependent on the ratio x of $xLi_2MnO_3\cdot(1-x)LiNi_{1/3}Co_{1/3}Mn_{1/3}O_2$. It is well documented that a higher value (>1.2) of $I_{(003)}/I_{(104)}$ is an indicator of lower cation mixing between Li^+, Ni^{2+}, Co^{3+} and Mn^{4+} [31]. As shown in Table 2,

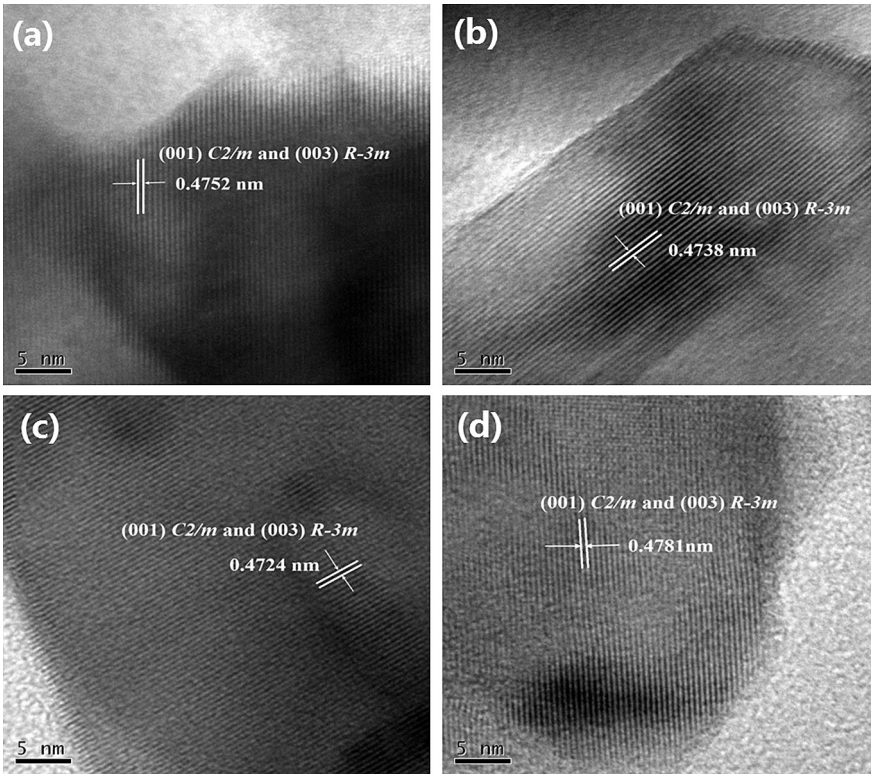

Fig. 3. HR-TEM of $xLi_2MnO_3\cdot(1-x)LiNi_{1/3}Co_{1/3}Mn_{1/3}O_2$ synthesized by microwave hydrothermal at 180 °C for 60 min with different ratio of x: (a) 0.2,(b) 0.4, (c) 0.6 and (d) 0.8.

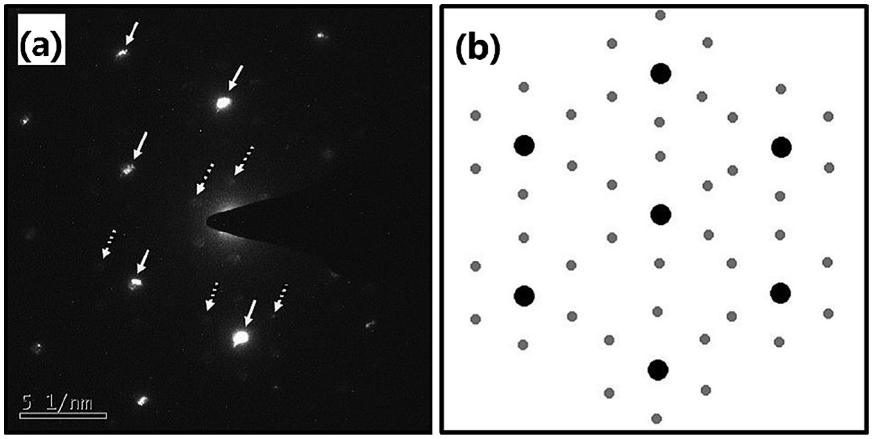

Fig. 4. (a) Selected area electron diffraction (SAED) of the sample 0.4LMO/LNCM_180C/60m and (b) superimposed rhombohedral and monoclinic reflections. (Solid arrow: strong reflections; dotted arrow: weak reflections).

the intensity ratios of $I_{(003)}/I_{(104)}$ are 1.05, 1.27, 1.15 and 0.89 in the samples $xLi_2MnO_3\cdot(1-x)LiNi_{1/3}Co_{1/3}Mn_{1/3}O_2$ with $x = 0.2$, 0.4, 0.6 and 0.8, respectively. The material with $x = 0.4$ has the lowest amount of cation mixing due to the bigger value of $I_{(003)}/I_{(104)}$, indicating the proper ratio x is very important for the good composition of $xLi_2MnO_3\cdot(1-x)LiNi_{1/3}Co_{1/3}Mn_{1/3}O_2$.

The XRD refinements by the Rietveld method with General Structure Analysis Software (GSAS Los Alamos National Laboratory, USA) and the refined lattice parameters are shown in Fig. 1 and listed in Table 2. Because the complex structure of $xLi_2MnO_3\cdot(1-x)LiNi_{1/3}Co_{1/3}Mn_{1/3}O_2$ which contains crystallographic sites shared by more than two cations, it is hard to obtain reliable results on atomic occupancies from the Rietveld refinement. In several previous publications, the composite $Li_2MnO_3/LiMO_2$ are always refined by α-$NaFeO_2$ type with R-3m, or monoclinic unit cell, C 2/m characterized Li_2MnO_3 [32,33]. In this work, the XRD patterns of the as-synthesized samples are refined by two sets of diffraction data. One set of strong and well-defined peaks can be readily identified to the α-$NaFeO_2$ type structure of the rhombohedral system with a space group R-3m. The other set of weak superstructure reflections between 20° and 25° can be ascribed to Li_2MnO_3 with a space group, $C2/m$. Since the reliability factor of χ^2 is less than 3, and the weighted factor of R_{wp}, R_p are less than 10%, the Rietveld refinement results are reliable.

As listed in Table 2, the cell parameters of both phase present minor change and depend on the ratio of $xLi_2MnO_3\cdot(1-x)LiNi_{1/3}Co_{1/3}Mn_{1/3}O_2$. For example, the cell parameter a by α-$NaFeO_2$ type with R-3m are 2.8614, 2.8638, 2.8578, and 2.8544 Å in $xLi_2MnO_3\cdot(1-x)LiNi_{1/3}Co_{1/3}Mn_{1/3}O_2$ with $x = 0.2$, 0.4, 0.6 and 0.8, respectively. The almost same values of c/a and cell volume indicate the cell structures could be kept at various ratio x in $xLi_2MnO_3\cdot(1-x)LiNi_{1/3}Co_{1/3}Mn_{1/3}O_2$. By comparison, $xLi_2MnO_3\cdot(1-x)LiNi_{1/3}Co_{1/3}Mn_{1/3}O_2$ refined by α-$NaFeO_2$ type with R-3m shows that the c/a value and cell volume quite depends on the ratio of x [34].

Fig. 2 shows the scanning electron microscopy of $xLi_2MnO_3\cdot(1-x)LiNi_{1/3}Co_{1/3}Mn_{1/3}O_2$ ($x = 0.2$, 0.4, 0.6, 0.8, respectively). All the materials show irregular agglomeration and the estimated average diameter is about 4–5 μm, which are a little different from the previous report of $Li_{1.15}[(Ni_{1/3}Co_{1/3}Mn_{1/3})_{0.5}(Ni_{1/4}Mn_{3/4})_{0.5}]_{0.85}O_2$ synthesized by the co-precipitation method using Na_2CO_3 as precipitant [35]. This phenomenon is possibly attributed to the precipitant used in precursor and the fast crystal growth mechanism of microwave-assisted hydrothermal process. The samples are comprised of agglomerates of nano-sized primary particles due to the rapid crystal formation in dozens minutes. The samples with $x = 0.2$, 0.6, 0.8 show the big distribution of particle size. As shown in Fig. 2b and the inset image, the morphology of the sample $x = 0.4$ presents relatively regular nanoparticles in high magnification, and sphere-like nanoclusters of the samples crystallites in smaller magnification.

Fig. 3 shows the HRTEM images of as-synthesized $xLi_2MnO_3\cdot(1-x)LiNi_{1/3}Co_{1/3}Mn_{1/3}O_2$ under different molar ratio of $Li_2MnO_3/LiMO_2$ (x). The calculated distance between two lattice fringes of the four samples with different ratio $x = 0.2$, 0.4, 0.6, 0.8 are 0.4752, 0.4738, 0.4724, 0.4781 nm, respectively, which corresponds to (003) planes from the rhombohedral phase and/or (001) planes from the monoclinic phase. The lattice fringe of the sample ($x = 0.4$) is close to the ideal interplanar distance of (003) plane of

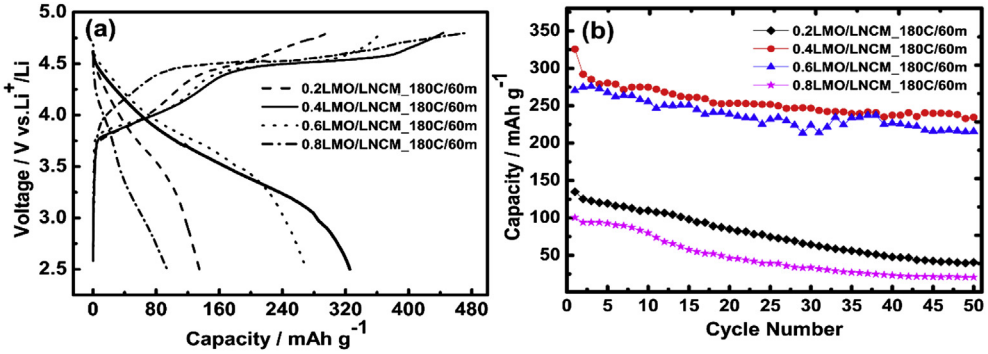

Fig. 5. The first charge/discharge profiles (a) and cycling performance (b) of the samples obtained via microwave hydrothermal at 180 °C for 60 min.

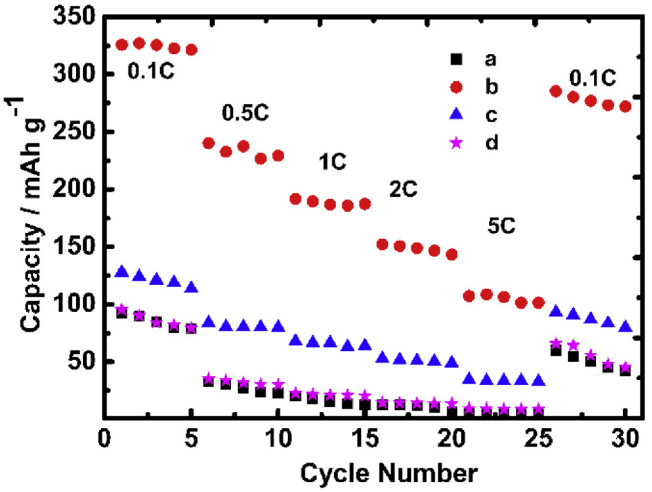

Fig. 6. Rate capability of $xLi_2MnO_3\cdot(1-x)LiNi_{1/3}Co_{1/3}Mn_{1/3}O_2$ obtained by microwave hydrothermal at 180 °C for 60 min with different ratio of x: (a) 0.2, (b) 0.4, (c) 0.6 and (d) 0.8.

the hexagonal layered phase $LiMO_2$ or [001] planes of a monoclinic Li_2MnO_3-like component.

The single crystal selected area electron diffraction (SAED) of the sample of 0.4LMO/LNCM_180C60m is shown in Fig. 4. The experimental SAED pattern consists of two sets of reflections; 1) the strong reflections (marked as solid arrow) could be indexed to rhombohedral phase, which often designated as O3 reflections where the lithium ions occupy the octahedral interstitial position in the unit cell [36]; 2) the weak reflections (marked as dotted arrow) could be uniquely treated as the monoclinic ($C2/m$) Li_2MnO_3-like component, which is visible in the Rietveld refinement of XRD patterns (as shown in Fig. 1b, $x = 0.4$). These weak reflections illustrate the ordering of lithium with the transition metal ion (Mn ions) in the transition metal layer. The inset image Fig. 4b shows simulated pattern of superimposed rhombohedral and monoclinic reflections with the O3 reflections, in agreement with the experimental SAED pattern. All the results of SAED confirm that the as-synthesized $xLi_2MnO_3\cdot(1-x)LiNi_{1/3}Co_{1/3}Mn_{1/3}O_2$ is the integration of Li_2MnO_3 and $LiNi_{1/3}Co_{1/3}Mn_{1/3}O_2$ [36,37].

Fig. 5 presents the initial charge/discharge profiles and cycling performance of $xLi_2MnO_3\cdot(1-x)LiNi_{1/3}Co_{1/3}Mn_{1/3}O_2$ with $x = 0.2$, 0.4, 0.6, 0.8 obtained through microwave hydrothermal at 180 °C for 60 min. All the materials exhibited two plateaus during the first charge, which are located at 3.7–4.5 V and above 4.5 V. The first plateau is attributed to lithium ion extraction from $LiNi_{1/3}Co_{1/3}Mn_{1/3}O_2$ phase corresponding to the oxidation of $Ni^{2+} \rightarrow Ni^{4+}$ and $Co^{3+} \rightarrow Co^{4+}$ [38]. The second plateau is considered to be the Li_2O taking off from the layered Li_2MnO_3 structure, which results in high irreversible charge capacity (more than 400 mA h g^{-1}) [39].

As shown in Fig. 5a, the initial discharge capacities are 134.9, 325.6, 270.4 and 94 mA h g^{-1} in $xLi_2MnO_3\cdot(1-x)LiNi_{1/3}Co_{1/3}Mn_{1/3}O_2$ with $x = 0.2$, 0.4, 0.6 and 0.8, respectively. The sample $0.8Li_2MnO_3\cdot0.2LiNi_{1/3}Co_{1/3}Mn_{1/3}O_2$ with the highest component of Li_2MnO_3 presents the lowest capacity and the most irreversible capacity value (378.6 mA h g^{-1}) due to the poor conductivity by the higher Mn^{4+} content and the large amount of Li_2O extraction [34]. The sample $0.2Li_2MnO_3\cdot0.8LiNi_{1/3}Co_{1/3}Mn_{1/3}O_2$ with the lowest component of Li_2MnO_3 also presents big irreversible charge/discharge capacity (296.8/134.9 mA h g^{-1}), and the low discharge capacity due to the overcharge of the major $LiNi_{1/3}Co_{1/3}Mn_{1/3}O_2$ component at upper cut-off voltage of 4.8 V. The capacity and cycling stability of the Li-rich material $xLi_2MnO_3\cdot(1-x)LiNi_{1/3}Co_{1/3}Mn_{1/3}O_2$ depend on the synergistic effect of Li_2MnO_3 (R-3m) and $LiNi_{1/3}Co_{1/3}Mn_{1/3}O_2$ ($C2/m$). For example, the previous publication of Li-rich material synthesized by traditional hydrothermal present the best capacity at proper x instead of the highest value of x [34]. The sample of 0.4LMO/LNCM_180C/60m with proper component of Li_2MnO_3 (R-3m) and $LiNi_{1/3}Co_{1/3}Mn_{1/3}O_2$ ($C2/m$), delivers the highest capacity and good initial reversibility (73.3%). The cycling performance of the samples with different ratio (x) is shown in

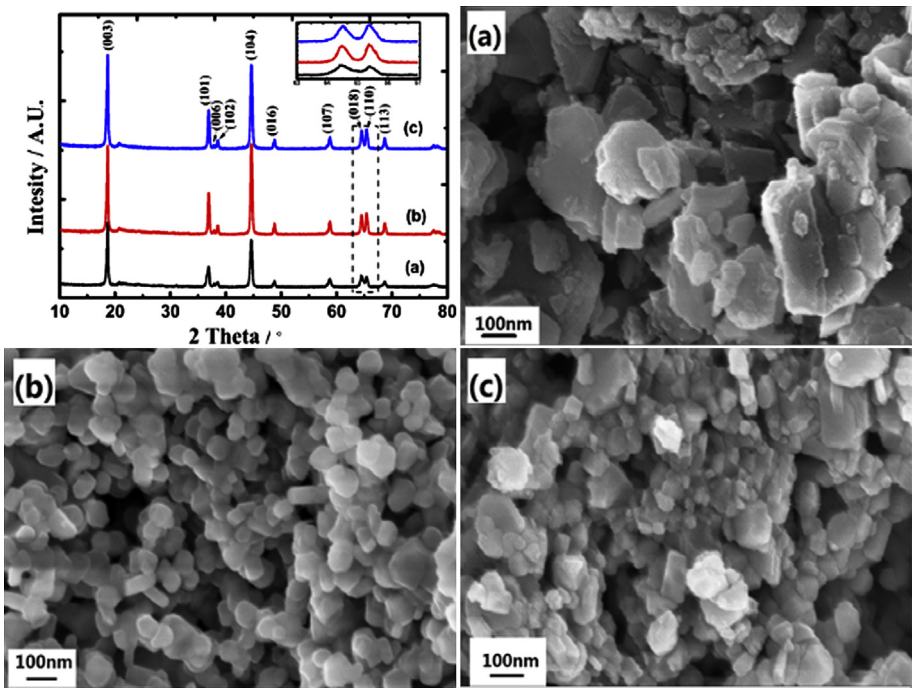

Fig. 7. X-ray diffraction patterns and SEM images of $xLi_2MnO_3\cdot(1-x)LiNi_{1/3}Co_{1/3}Mn_{1/3}O_2$ ($x = 0.4$) at constant microwave hydrothermal temperature: (a) 160, (b) 180 and (c) 200 °C.

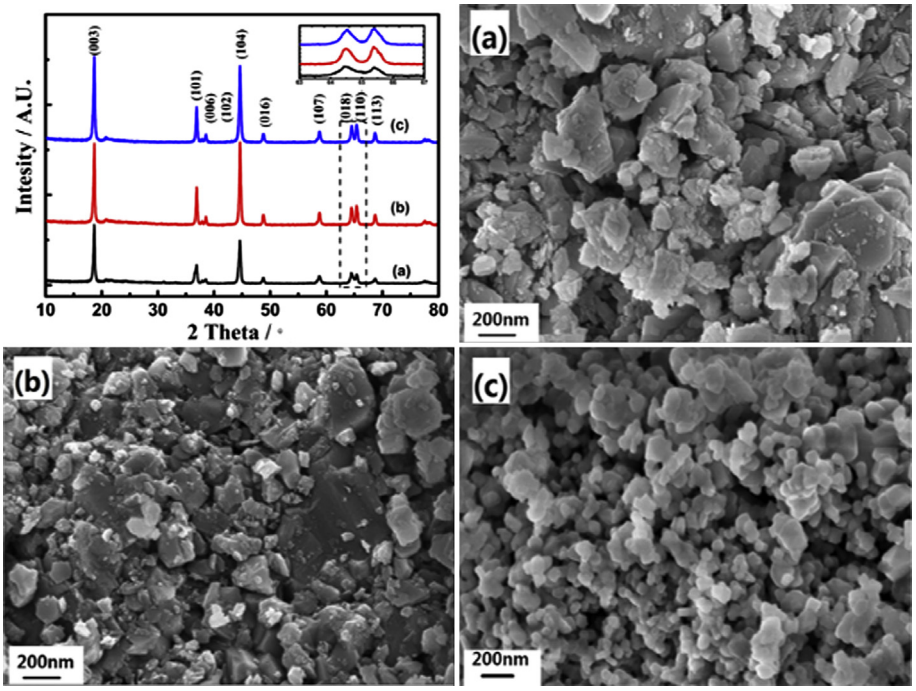

Fig. 8. X-ray diffraction patterns and SEM images of $x\mathrm{Li_2MnO_3}\cdot(1-x)\mathrm{LiNi_{1/3}Co_{1/3}Mn_{1/3}O_2}$ ($x = 0.4$) at 180 °C for different microwave hydrothermal time: (a) 30, (b) 45 and (c) 60 min.

Fig. 5a. The samples of 0.4LMO/LNCM_180C/60m and 0.6LMO/LNCM_180C/60m exhibited good capacity retention within 50 cycles.

The cells of $x\mathrm{Li_2MnO_3}\cdot(1-x)\mathrm{LiNi_{1/3}Co_{1/3}Mn_{1/3}O_2}$ materials with different x were charged/discharged at different current densities (0.1, 0.5, 1, 2, and 5 C) as shown in Fig. 6. Along with the current density increases, all the samples showed gradual loss of discharge capacity. The sample 0.4LMO/LNCM180C/60m delivers 325.7, 240.2, 191.5, 152.1, 107.2 mA h g^{-1} at the current densities of 0.1 C, 0.5 C, 1 C, 2 C, and 5 C, respectively. The results are better than that of materials synthesized under the conventional method, such as high temperature solid-state and conventional hydrothermal method [40,41]. As can be observed in Fig. 6a, the sample of 0.4LMO/LNCM_180C/60m still maintains higher capacity (87.6% of the initial discharge capacity) at 0.1 C again, after it cycled at different rates up to 5 C. The proper composition of $\mathrm{Li_2MnO_3}$ plays an important role to improve the capacity and stability of the Li-rich cathode material [42]. In the following discussion, the crystal structure, morphology and electrochemical properties of 0.4LMO/LNCM_180C/60m are studied in detail.

Fig. 7 shows the XRD patterns and SEM of $0.4\mathrm{Li_2MnO_3}\cdot0.6\mathrm{LiNi_{1/3}Co_{1/3}Mn_{1/3}O_2}$ synthesized at different microwave hydrothermal temperature. All the XRD patterns (in Fig. 7) are indexed to a unit cell of α-$\mathrm{NaFeO_2}$ type with space group R-3m and the weak peaks at $2\theta = 20–25°$ indexed to monoclinic unit cell, $C2/m$, that characterizes $\mathrm{Li_2MnO_3}$. As shown in the inset images of the XRD pattern, more clear splits of (018)/(110) are observed in the sample 0.4LMO/LNCM_180C/60m, compared with those in the samples of 0.4LMO/LNCM_160C/60m and 0.4LMO/LNCM_200C/60m. As shown in Fig. 7a–c, the general appearance of the three samples are high crystalline. The particles synthesized at 180 °C are more homogenous and smaller, which are assembled from the sphere-like primary grains with a diameter of 100 nm. At the microwave hydrothermal temperature of 160 °C, the reactants might be not sufficient to react, but at high temperature of 200 °C, the grains happen to grow big and present big crystal size distribution. The average crystal size of the samples obtained at 200 °C are approximately 50–150 nm (as shown in Fig. 7c).

Fig. 8 shows the XRD patterns and SEM of $0.4\mathrm{Li_2MnO_3}\cdot0.6\mathrm{LiNi_{1/3}Co_{1/3}Mn_{1/3}O_2}$ synthesized at different microwave hydrothermal time. Compared with the XRD patterns of TH_0.4LMO/LNCM_180C/48h (as shown Fig. S1a in Support information), the sample synthesized under MH 30 min and 45 min show broad and weak diffraction peaks (Fig. 8a), due to without enough time forming ordered phases. As shown in the inset image of XRD pattern, the peak separation of (018) and (110) reflections at 64–66° became clearer with the increasing of MH time, indicating that the cation disordering between lithium and metal ions are reduced. The pure phase of $0.4\mathrm{Li_2MnO_3}\cdot0.6\mathrm{LiNi_{1/3}Co_{1/3}Mn_{1/3}O_2}$ could be obtained in a very short MH time of 30 min, but the crystal morphology (as

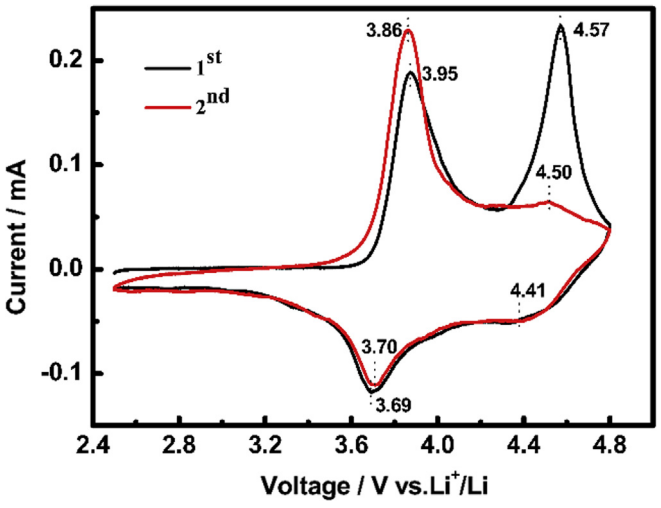

Fig. 9. Cyclic voltammograms of 0.4LMO/LNCM_180C/60m material at the scan rate of 0.1 mV s^{-1} in a potential range of 2.5–4.8 V (vs. Li^+/Li).

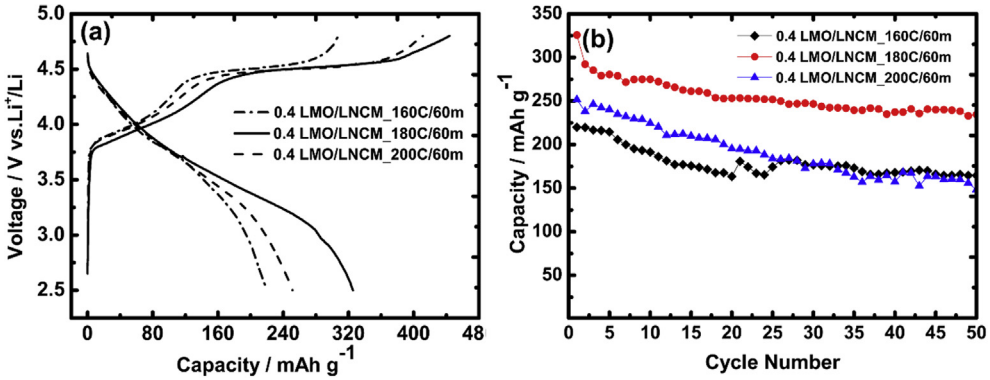

Fig. 10. The initial charge/discharge profiles (a) and cycle performance (b) of $0.4Li_2MnO_3{\cdot}0.6LiNi_{1/3}Co_{1/3}Mn_{1/3}O_2$ obtained for 60 min at different microwave hydrothermal temperature: 160, 180 and 200 °C, respectively.

shown in Fig. 8a, b) is big irregular particles with big crystal size distribution. Along with the increasing of microwave hydrothermal time, the particles of the samples grow much homogeneous and present higher crystallinity morphology.

Fig. 9 shows the cyclic voltammetry (CV) curves recorded for the sample 0.4LMO/LNCM_180C/60m during the first two cycles. The curves are well-defined and present widened oxidation/reduction peaks, which is representative of the kinetic process regarding to the diffusion of lithium ion in a solid phase and electron jumping across the electrode. The sample presents two couples of oxidation and reduction peaks between 2.5 and 4.8 V. In the initial anodic process, two oxidation peaks appear at 3.95 V and 4.57 V (vs. Li^+/Li), respectively. The former is attributed to the extraction of lithium ion from $LiMO_2$ structure, corresponding to the oxidation of Ni^{2+} and Co^{3+}. The latter is attributed to the removal of lithium ion from Li_2MnO_3 structure accompanied with the coinstantaneous oxygen evolution [43]. In the following cathodic process, a strong peak observed at 3.69 V is attributed to the reinsertion of Li to $Li_{1-x}MO_2$ structure, and a minor peak at 4.41 V is attributed to Li reinsertion to the activated *C*2/*m* structure of $Li_{2-x}MnO_3$ [24]. In the second CV cycle, the redox peaks present good overlap except the almost disappeared oxidation peak at 4.57 V. It might be due to the fact that the removal of lithium ion from Li_2MnO_3 structure accompanied with the coinstantaneous oxygen evolution is irreversible in the first CV process, which is well agree with the common irreversible capacity of Li-rich cathodes [39].

Fig. 10 shows the initial charge/discharge curves and cycle performance of $0.4Li_2MnO_3{\cdot}0.6LiNi_{1/3}Co_{1/3}Mn_{1/3}O_2$ obtained at 160, 180 and 200 °C, which deliver the initial capacity 219.9, 325.6, and 251.5 mA h g^{-1}, respectively. The lowest and the highest MH temperatures led to irregular nanoparticles and big particle size distribution (as shown in Fig. 7a and c), while the as-synthesized samples present low capacities. With respect to the cycling performance (Fig. 10b), it is can be observed that the capacities of 0.4LMO/LNCM_160C/60m and 0.4LMO/LNCM_200C/60m dropped to 176.6 and 177.9 mA h g^{-1} after 50 cycles at 0.1 C, but 0.4LMO/LNCM_180C/60m remained 246.7 mA h g^{-1}. Proper MH temperature (180 °C) is important in the particle size and size distribution, which further affect their electrochemical properties.

MH time is another factor in the electrochemical properties of the obtained products. The initial charge/discharge profiles and cycling performance of $0.4Li_2MnO_3{\cdot}0.6LiNi_{1/3}Co_{1/3}Mn_{1/3}O_2$ synthesized at 180 °C for various MH time are shown in Fig. 11. As shown in Fig. 11a, the charge and discharge capacity raised along with the increasing MH time, 225.5, 253.0 and 325.6 mA h g^{-1} for the samples obtained for 30, 45 and 60 min, respectively. Moreover, shorter MH time is not sufficient for the sample $0.4Li_2MnO_3{\cdot}0.6LiNi_{1/3}Co_{1/3}Mn_{1/3}O_2$ to grown homogeneous particles. For 60 min of MH reaction time, the as-synthesized samples present smaller particle size and higher crystalline (as shown in Fig. 8a and b) and present the best initial discharge capacity and cycle performance. After 50 charge/discharge cycles, the discharge capacities remain 133.4, 128.8, 234.5 mA h g^{-1} in the samples obtained at 180 °C for 30, 45 and 60 min, respectively. But TH_0.4LMO/LNCM_180C/48h synthesized for 48 h by traditional hydrothermal present poor electrochemical properties (as shown Fig. 1c in Support information), such as the initial capacity of 200 mA h g^{-1} and remaining 156 mA h g^{-1} at the 50th cycle.

Fig. 12 shows the effects of MH parameters in the $0.4Li_2MnO_3{\cdot}0.6LiNi_{1/3}Co_{1/3}Mn_{1/3}O_2$ cathode material on the rate capability.

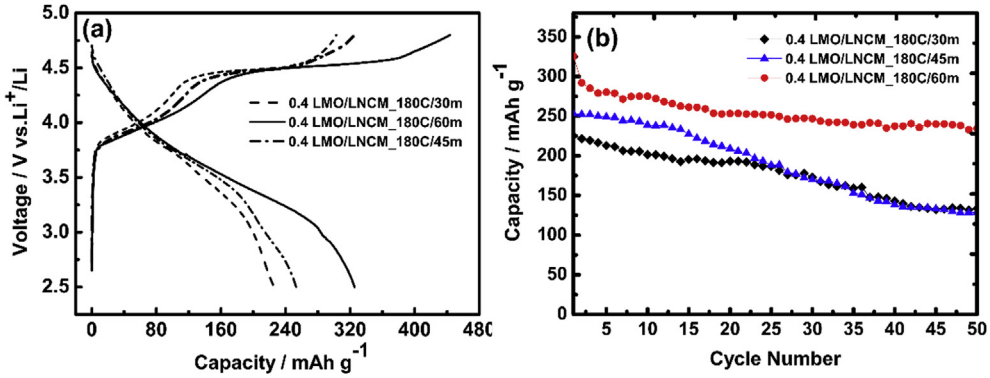

Fig. 11. The initial charge/discharge profiles (a) and cycle performance (b) of $0.4Li_2MnO_3{\cdot}0.6LiNi_{1/3}Co_{1/3}Mn_{1/3}O_2$ obtained at 180 °C for different microwave hydrothermal time: 30, 45 and 60 min, respectively.

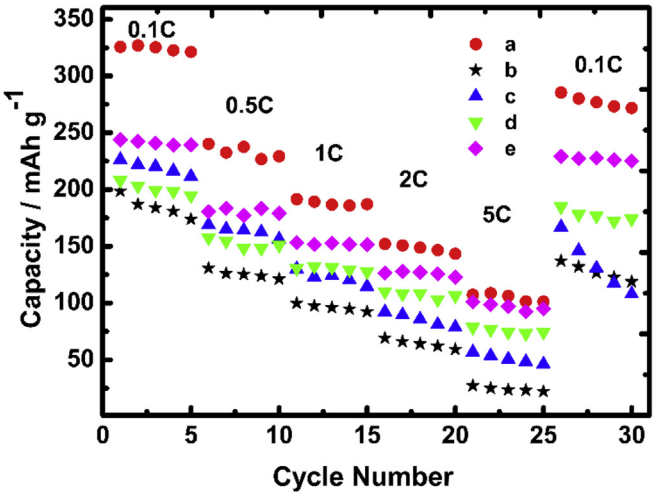

Fig. 12. Rate capability of $xLi_2MnO_3\cdot(1-x)LiNi_{1/3}Co_{1/3}Mn_{1/3}O_2$ ($x = 0.4$) obtained in different MH conditions: (a) 180 °C for 60 min, (b) 160 °C for 60 min, (c) 180 °C for 45 min, (d)180 °C for 30 min, and (e) 200 °C for 60 min.

All the samples synthesized under various MH temperatures and times are charged and discharged at 0.1, 0.5, 1, 2 and 5 C, respectively. Both MH temperature and time have the effect in the $0.4Li_2MnO_3\cdot0.6LiNi_{1/3}Co_{1/3}Mn_{1/3}O_2$ cathode material on the rate capability. For example, the sample synthesized at 180 °C for 60 min presents the highest capacity of 107.2 mA h g^{-1} at 5 C rate, and still remain discharge capacity of 285.3 mA h g^{-1} at the return back to 0.1 C rate after the charge/discharge from 0.1 C to 5 C for 25 cycles.

4. Conclusions

A series of layered $xLi_2MnO_3\cdot(1-x)LiNi_{1/3}Co_{1/3}Mn_{1/3}O_2$ ($x = 0.2$, 0.4, 0.6, 0.8) cathode materials were synthesized successfully by microwave-assisted hydrothermal method in a short time (30–60 min). The MH conditions, such as temperature and time, are systematically optimized. Rietveld refinement of XRD patterns and HRTEM indicate that all the samples could be indexed to monoclinic ($C2/m$) Li_2MnO_3-like component and trigonal (R-3m) $LiMO_2$ component. SEM shows the sample prepared under the condition of MH180 °C/60 min with $x = 0.4$ appears spherical micro-particles morphology composed of primary spherical nanoparticles with a diameter of 50–100 nm. The charge/discharge results demonstrate that the sample 0.4LMO/LNCM_180C/60m delivers a high initial capacity of 325 mA h g^{-1} at 0.1 C in the voltage range of 2.5–4.8 V and remains 234.5 mA h g^{-1} after 50 cycles. When the current density increased to 0.5 C, 1 C, 2 C and 5 C, the maximum discharge capacities are 240.2, 191.5, 152.1 and 107.2 mA h g^{-1}, respectively. Microwave-assisted hydrothermal synthesis of Li-rich cathode material might open a new approach for the development of advanced lithium ion batteries with high energy density, long cycle life and good rate performance.

Acknowledgments

The authors acknowledge the supports of the 085 Project of Shanghai Education Commission, Instrumental Analysis and Research Center of Shanghai University, NSF of Jiangsu Province of China (Grant No. BK2010262), NSF of Jiangsu Educational Department of China (Grant No. 10KJA480001), and NSF of China (Grant No. 51172032).

Appendix A. Supplementary data

Supplementary data related to this article can be found at http://dx.doi.org/10.1016/j.jpowsour.2013.08.097.

References

[1] J.M. Tarascon, M. Armand, Nature 414 (2001) 359–367.
[2] H.-K. Song, K.T. Lee, M.G. Kim, L.F. Nazar, J. Cho, Adv. Funct. Mater. 20 (2010) 3818–3834.
[3] X. Zhang, C. Yu, X. Huang, J. Zheng, X. Guan, D. Luo, L. Li, Electrochim. Acta 81 (2012) 233–238.
[4] J. Li, R. Klöpsch, M.C. Stan, S. Nowak, M. Kunze, M. Winter, S. Passerini, J. Power Sources 196 (2011) 4821–4825.
[5] A. Ito, D. Li, Y. Sato, M. Arao, M. Watanabe, M. Hatano, H. Horie, Y. Ohsawa, J. Power Sources 195 (2010) 567–573.
[6] B. Huang, Y.-I. Jang, Y.-M. Chiang, D.R. Sadoway, J. Appl. Electrochem. 28 (1998) 1365–1369.
[7] L.X. Yuan, Z.H. Wang, W.X. Zhang, X.L. Hu, J.T. Chen, Y.H. Huang, Energy Environ. Sci. 4 (2011) 269–284.
[8] K.M. Shaju, G.V. Subba Rao, B.V.R. Chowdari, Electrochim. Acta 48 (2002) 145–151.
[9] J.T. Son, H.J. Jeon, J.B. Lim, Adv. Powder Technol. 24 (2013) 270–274.
[10] K.A. Jarvis, Z. Deng, L.F. Allard, A. Manthiram, P.J. Ferreira, Chem. Mater. 23 (2011) 3614–3621.
[11] H. Koga, L. Croguennec, M. Ménétrier, P. Mannessiez, F. Weill, C. Delmas, J. Power Sources 236 (2013) 250–258.
[12] A.R. Armstrong, M. Holzapfel, P. Novak, C.S. Johnson, S.-H. Kang, M.M. Thackeray, P.G. Bruce, J. Am. Chem. Soc. 128 (2006) 8694–8698.
[13] J. Bareño, C.H. Lei, J.G. Wen, S.-H. Kang, I. Petrov, D.P. Abraham, Adv. Mater. 22 (2010) 1122–1127.
[14] M.M. Thackeray, S.H. Kang, C.S. Johnson, J.T. Vaughey, R. Benedek, S.A. Hackney, J. Mater. Chem. 17 (2007) 3112–3125.
[15] C.R. Fell, D.H. Lee, Y.S. Meng, J.M. Gallardo-Amores, E. Moran, M.E. Arroyo-de Dompablo, Energy Environ. Sci. 5 (2012) 6214–6224.
[16] J. Breger, Y.S. Meng, Y. Hinuma, S. Kumar, K. Kang, Chem. Mater. 18 (2006) 4768–4781.
[17] S.J. Shi, J.P. Tu, Y.Y. Tang, Y.X. Yu, Y.Q. Zhang, X.L. Wang, J. Power Sources 221 (2013) 300–307.
[18] O. Toprakci, H.A.K. Toprakci, Y. Li, L.W. Ji, L.G. Xue, H. Lee, S. Zhang, X.W. Zhang, J. Power Sources 241 (2013) 522–528.
[19] S. Kang, M. Thackery, Electrochem. Commun. 11 (2009) 748–751.
[20] J. Wang, B. Qiu, H.L. Cao, Y.Y. Xia, Z.P. Liu, J. Power Sources 218 (2012) 128–133.
[21] J.-H. Lim, H. Bang, K.-S. Lee, K. Amine, Y.-K. Sun, J. Power Sources 189 (2009) 571–575.
[22] J. Liu, B.R. Jayan, A. Manthiram, J. Phys. Chem. C 114 (2010) 9528–9533.
[23] M. Tabuchi, A. Nakashima, K. Ado, H. Kageyarna, K. Tatsumi, Chem. Mater. 17 (2005) 4668–4677.
[24] J.-H. Jeong, B.-S. Jin, W.-S. Kim, G. Wang, H.-S. Kim, J. Power Sources 196 (2011) 3439–3442.
[25] J.-H. Kim, C.W. Park, Y.-K. Sun, Solid State Ionics 164 (2003) 43–49.
[26] X. Huang, Q. Zhang, H. Chang, J. Gan, H. Yue, Y. Yang, J. Electrochem. Soc. 156 (2009) A162–A168.
[27] H.M. Ji, G. Yang, X.W. Miao, A.Q. Hong, Electrochim. Acta 55 (2010) 3392–3397.
[28] A. Vadivel Murugan, T. Muraliganth, A. Manthiram, J. Electrochem. Soc. 156 (2009) A79–A83.
[29] G. Yang, H.M. Ji, H.D. Liu, J. Nanosci. Nanotechnol. 10 (2010) 980–986.
[30] A.C. Larson, R.B. Von Dreele, General Structure Analysis System (GSAS), Los Alamos National Laboratory, 2000, pp. 86–748. Report LAUR.
[31] T. Ohzuku, A. Ueda, M. Nagayama, J. Electrochem. Soc. 140 (1993) 1862–1870.
[32] N. Yabuuchi, K. Yoshii, S.T. Myung, I. Nakai, S. Komaba, J. Am. Chem. Soc. 133 (2011) 4404–4419.
[33] C. Yu, H. Wang, X. Guan, J. Zheng, L. Li, J. Alloys Compd. 546 (2013) 239–245.
[34] X. Guo, Y. Li, M. Zheng, J. Zheng, J. Li, Z. Gong, Y. Yang, J. Power Sources 184 (2008) 414–419.
[35] X. Yang, X. Wang, Q. Wei, H. Shu, L. Liu, S. Yang, B. Hu, Y. Song, G. Zou, L. Hu, L. Yi, J. Mater. Chem. 22 (2012) 19666–19672.
[36] M.M. Thackeray, S.H. Kang, C.S. Johnson, J.T. Vaughey, S.A. Hackney, Electrochem. Commun. 8 (2006) 1531–1538.
[37] D. Mohanty, S. Kalnaus, R.A. Meisner, K.J. Rhodes, J. Li, E.A. Payzant, D.L. Wood, C. Daniel, J. Power Sources 229 (2013) 239–248.
[38] M.M. Thackeray, C.S. Johnson, J.T. Vaughey, N. Li, S.A. Hackney, J. Mater. Chem. 15 (2005) 2257–2267.
[39] C.S. Johnson, N. Li, C. Lefief, J.T. Vaughey, M.M. Thackeray, Chem. Mater. 20 (2008) 6095–6106.
[40] D. Kim, J. Gim, J. Lim, S. Park, J. Kim, Mater. Res. Bull. 45 (2010) 252–255.
[41] M. Tabuchi, Y. Nabeshima, M. Shikano, K. Ado, H. Kageyama, K. Tatsumi, J. Electrochem. Soc. 154 (2007) A638–A648.
[42] S.J. Shi, J.P. Tu, Y.Y. Tang, Y.Q. Zhang, X.L. Wang, C.D. Gu, J. Power Sources 240 (2013) 140–148.
[43] S.J. Shi, J.P. Tu, Y.Y. Tang, Y.X. Yu, Y.Q. Zhang, X.L. Wang, C.D. Gu, J. Power Sources 228 (2013) 14–23.